Acta Geotechnica
https://doi.org/10.1007/s11440-023-01907-3

RESEARCH PAPER

# Experimental study with complete stress state interpretation of undrained monotonic and cyclic simple shear tests with flexible boundaries

L. Mele[1]

Received: 9 February 2022 / Accepted: 19 April 2023


**Abstract**
In many geotechnical problems, the stress state may be approximated by a simple shear stress state. Owing to that, simple shear tests, in which the principal axes of stresses and strains are free to rotate, should be preferred to investigate the soil mechanical behaviour. However, the most common simple shear devices (rigid boundaries) do not allow to completely know the stress state of the specimen. Therefore, the interpretation of this test type has always been developed only theoretically. In order to improve the basic understanding of simple shear stress paths, a more innovative simple shear device with flexible boundaries was used in this research. The specimen is enclosed with an unreinforced membrane and confined by cell pressure. The diameter is kept constant through a sophisticated control system, which well approximates a $K_0$ condition. The undrained monotonic and cyclic simple shear tests on an Italian sand are presented and discussed. Based on some hypotheses, the stress state is reasonably determined and represented by Mohr's circles. The theoretical interpretations show that the soil failure—under monotonic and cyclic loading—is reached when the effective intermediate principal stress is midway between the major and minor principal effective stresses ($b = 0.5$; $\theta = 0$), while the principal stress directions tend to reach a slope of 45°. Finally, the mechanical response of the tested sand is compared with the results of triaxial tests from a static and cyclic point of view. In agreement with several results reported in the literature, the friction angle in critical state conditions is higher in simple shear tests compared to that achieved in triaxial tests due to the rotation of principal stress directions. Moreover, the results of cyclic simple shear tests, in terms of liquefaction resistance ($CRR_{15} \approx 0.13$), are consistent with those performed in cyclic triaxial conditions.

**Keywords** Flexible boundaries · Liquefaction · Rotation of principal stress directions · Simple shear tests

## 1 Introduction

For measuring the strength and stiffness of the soil, laboratory testing is widely used. Although triaxial tests are simple enough and rather common, the direct simple shear (DSS) tests—or simply simple shear tests—should be preferred. In addition to hollow cylinder/torsional shear test, simple shear test subjects the soil specimen to constant-volume plane-strain conditions and allows principal stresses rotation. These stress conditions are useful for modelling soil response to earthquake loading and liquefaction phenomena [28], shearing adjacent to a pile shaft [29] or under offshore foundation systems [2]. An ideal simple shear stress condition, with the application of uniform shear stress ($\delta\tau_{zy}$), should impose $\delta\varepsilon_{xx} = \delta\varepsilon_{yy} = \delta\varepsilon_{zz} = \delta\gamma_{xy} = \delta\gamma_{xz} = 0$, with $\delta\gamma_{zy} \neq 0$ (Fig. 1). Historically, the two most common types of simple shear apparatus are those developed by the University of Cambridge [30] and the Norwegian Geotechnical Institute (NGI) [1, 7]. Both are improvement to the first direct shear device developed at Royal Swedish Geotechnical Institute (SGI) [16] that used cylindrical specimens confined by stacked rings. Cambridge device tests square specimens in a rigid box [8], which allows imposing the true $K_0$ condition ($\varepsilon_{xx} = \varepsilon_{yy} = \varepsilon_r = 0$). On the other hand, in the NGI apparatus cylindrical specimens are confined laterally by a wire-reinforced rubber membrane [8]. Nowadays, similar

✉ L. Mele
lucia.mele@unina.it

[1] University of Napoli Federico II, Naples, Italy

Published online: 18 May 2023

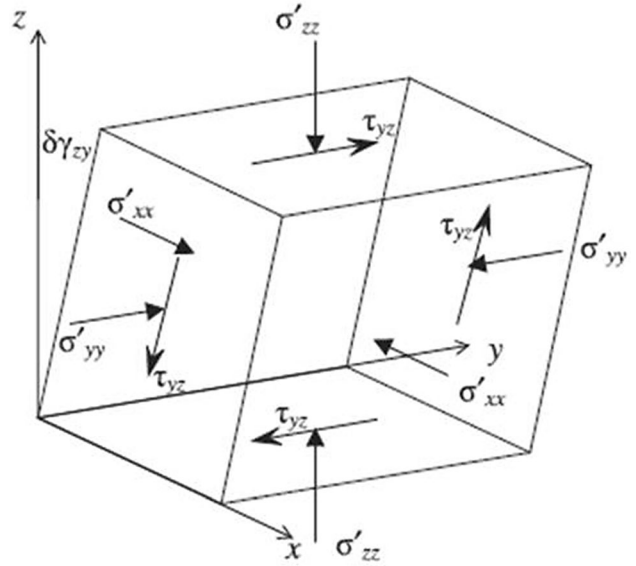


**Fig. 1** Stresses acting on an ideal simple shear element [13]

to SGI device [16], the wire-reinforced rubber membrane is replaced by stack frictionless rings [23, 34], which allow shear deformation but avoid any change of cross-sectional area.

More recently, further development of devices, using flexible boundaries, has been introduced. Among others, those developed at Berkeley [35] and University of Western Australia (UWA) [21] can be mentioned. Both of them use cylindrical specimens between rigid caps (top and bottom) and confined by unreinforced latex rubber membrane within a cell pressure. Horizontal and vertical stresses may be controlled independently, and the cross-sectional area may be maintained approximately constant. In this case, radial strains ($\varepsilon_r$) are low, but not nil.

Although DSS tests better represent the real behaviour of the soil when subjected to simple shear deformations, as reported by Doherty and Fahey [13], no DSS device can impose true simple shear conditions since a complex non-uniform stress state in the specimen makes the interpretation of the tests difficult. Non-uniform stress state is mainly due to the fact that frictionless vertical boundaries cannot develop the complementary shear stresses necessary for equilibrium. Lacking complementary frictional forces in the simple shear test creates a mechanically impermissible stress state for a single element [37]. Moreover, stress non-uniformities within the specimen can also be affected by the top-cap rotation (rocking), which violates the assumption that top and bottom faces remain parallel in simple shear deformation.

Budhu [8] studied in depth the non-uniformities imposed by simple shear devices. Using the radiographic technique, he showed that for shear strain less than 5%, there is a reasonable uniformity of strains. When shear strains exceed 5%, the square specimen (Cambridge apparatus) develops horizontal zone of preferential dilation near midheight. In contrast, in cylindrical specimen (NGI apparatus), zone of preferential dilation may be observed to begin at the top of the specimen spreading down to the right-hand corner. He demonstrated that the direction of rupture surface in soil laboratory specimens is influenced by the stiffness of the boundaries of the apparatus. In particular, Budhu [9] presented the results of X-ray tests on NGI specimens, showing that the angle to the horizontal planes of the rupture surface is about 14°. It is important to mention that the problem of boundary effects, and as a consequence non-uniformities of stress state of the specimens, can be reduced by testing specimens with low aspect ratio (= $h/d$, where $h$ is the height and $d$ is the diameter of the specimen) [36].

Since there are non-uniformities of the stress state of the specimen, the interpretation of this test type results is often complex. Generally, Cambridge and NGI tests are interpreted assuming that the horizontal planes are planes of maximum shear stress at large strains [31]. However, the approach of de Josselin de Jong [12] is also used. He proposed that the failure in simple shear could occur by either sliding on horizontal planes or sliding in conjunction with rotations on vertical planes. Both modes are equally possible, and the sample will choose the one with the least resistance. Simple shear tests with confining pressure (such as Berkeley and UWA) are more complex than the traditional devices (Cambridge and NGI) but allow to completely know the stress state of the specimen. However, their interpretation may be fairly complex, as well. After loading along a single shearing direction, the shape of the specimen changes from right cylinder to oblique cylinder. It means that horizontal stresses are not always equal to cell pressure. Moreover, no complementary shear stresses exist on the vertical boundaries. Starting from the equilibrium of the truncated oblique cylinder, Carraro [10] proposed a method to estimate more correctly the stress state of the specimens. He also demonstrated that the obtained results differ little from those obtained with the traditional interpretation of a right cylinder, which implies that the horizontal stress is equal to the cell pressure. According to him, the critical state conditions are well estimated considering the right cylinder.

The need to interpret the results of simple shear tests imposes to assume the hypotheses of (1) uniformity of stress state, (2) the consequent complementarity of shear stresses on the vertical planes of the specimen, and (3) the traditional interpretation of a right cylinder. Under the aforementioned hypotheses, the principal normal effective stresses ($\sigma'_1$, $\sigma'_2$, $\sigma'_3$) can be obtained from the following equations:

$$\sigma'_{1,3} = \frac{\sigma'_v + \sigma'_h}{2} \mp \sqrt{\left(\frac{\sigma'_v - \sigma'_h}{2}\right)^2 + \tau^2} \quad \sigma'_2 = \sigma'_h \tag{1}$$

where $\sigma'_1$, $\sigma'_2$ and $\sigma'_3$ are the maximum, intermediate and minimum principal normal effective stresses, respectively, $\sigma'_v$ and $\sigma'_h$ are the vertical and the horizontal effective stresses, respectively, and $\tau$ is the horizontal shear stress. This assumption allows to evaluate the two invariants: $p'$ (mean effective stress) and $q$ (deviatoric stress) in terms of principal effective stresses:

$$p' = \frac{1}{3} \cdot \left(\sigma'_1 + \sigma'_2 + \sigma'_3\right) \tag{2}$$

$$q = \frac{1}{\sqrt{2}} \cdot \sqrt{\left(\sigma'_1 - \sigma'_2\right)^2 + \left(\sigma'_1 - \sigma'_3\right)^2 + \left(\sigma'_2 - \sigma'_3\right)^2} \tag{3}$$

The third stress invariant is Lode's angle ($\theta$). It can be used to define the orientation of the stress state within the deviatoric plane and may be defined as:

$$\theta = \arctan\left[\frac{1}{\sqrt{3}} \cdot (2b - 1)\right] \tag{4}$$

where $b$ is the intermediate principal stress coefficient, defined as:

$$b = \frac{\sigma'_2 - \sigma'_3}{\sigma'_1 - \sigma'_3} \tag{5}$$

Randolph and Wroth [29] demonstrated theoretically that simple shear failure condition is reached when the effective intermediate principal stress is midway between the major and minor principal effective stresses (e.g. $\theta = 0$ and $b = 0.5$). On the contrary, in triaxial tests b is constant. It is 0 in compression tests ($\sigma'_2 = \sigma'_3$) and 1 in extension tests ($\sigma'_2 = \sigma'_1$). As a consequence, $\theta$ (Eq. 4) is $-30°$ and $30°$ in triaxial compression and extension tests, respectively.

In geotechnical design, the Mohr–Coulomb model of frictional strength is generally used. The Mohr–Coulomb failure criterion, for cohesionless soils, can be expressed in terms of stress invariant $p'$, $q$ and $\theta$:

$$q = \left(\frac{\sin\varphi'}{\frac{\cos\theta}{\sqrt{3}} + \frac{\sin\theta \cdot \sin\varphi'}{3}}\right) \cdot p' \tag{6}$$

The friction angle ($\phi'$) may be computed from Eq. (6) imposing Lode's angle equal to 0 (simple shear tests). This slope forms a tangent to the final Mohr's circle. If soils are deformed according to simple shear mode, the friction angle of the soil estimated by simple shear tests is generally more reliable than that obtained by compression triaxial tests, which are performed in b-constant conditions. Since no rotation of principal stress direction occurs, the friction angle of the soil could be underestimated in compression triaxial tests [17].

Due to the difficulties and limits of simple shear tests, their interpretation has been often done from a theoretical point of view. Generally, they are hardly even confirmed by experimental data because of the impossibility to completely know the stress states of the specimens, especially when rigid boundaries are used. In this paper, the experimental results of undrained monotonic and cyclic simple shear tests on an Italian sand performed in a simple shear device with flexible boundaries have allowed to investigate the simple shear stress state of soil and improve the basic understanding on simple shear stress paths. The simple shear device (University of Napoli Federico II) allows to impose a constant diameter during consolidation and shear phases through a sophisticated control system. Some limits (such as the unavoidable oscillations of specimen's diameter) and potentialities of this device have been carefully analysed and discussed. Moreover, theoretical interpretations have been presented. Starting from that, the Italian sand has been characterized further from a static and a cyclic point of view.

## 2 Materials and SS apparatus

### 2.1 Materials

Within the European Project LIQUEFACT, a wide experimental study was carried out in order to characterize the sandy soils coming from an area located in Emilia Romagna region, which was affected by extensive liquefaction phenomena during the 2012 earthquake in Northern Italy (Pieve di Cento—Bologna). In this paper, the experimental results of tests performed on Pieve di Cento sand are shown. Pieve di Cento sand has a greyish colour; hence, it was called as grey silty sand (GSS) by Mele et al. [24]. The grain size distribution curve and the physical properties of the tested soil are reported in Fig. 2 and Table 1, respectively.

### 2.2 SS apparatus (University of Napoli Federico II)

In this research, the sophisticated simple shear apparatus—made by VJ-Tech (www.vjtech.co.uk)—has been used. This apparatus tests cylindrical specimens ($d = 70$ mm; $h = 26$ mm) with $h/d < 0.4$, as stated by ASTM [5, 6] to reduce stress/strain non-uniformity effects. The device can work with a double configuration: with rigid and flexible boundaries. In the first case, the specimen is enclosed with rigid, frictionless rings (Fig. 3a). In the second one, it is enclosed with an unreinforced latex membrane confined by

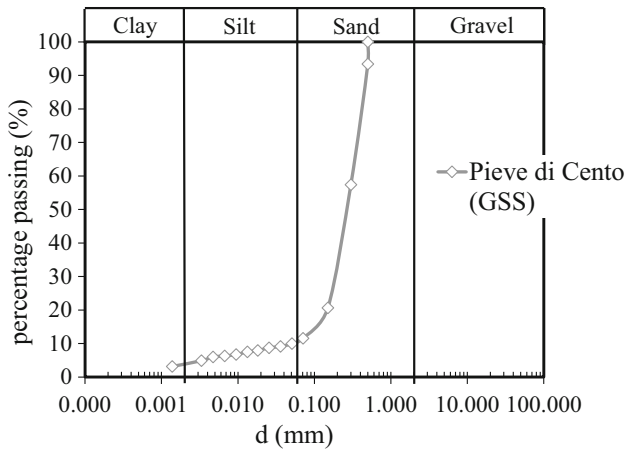


**Fig. 2** Grain size distribution curve of Pieve di Cento sand [24]

**Table 1** Physical properties of Pieve di Cento sand

| | |
|---|---|
| $G_s$ | 2.655 |
| $e_{max} - e_{min}$ | 0.884 – 0.442 |
| $D_{50}$ (mm) | 0.30 |
| $U_c$ | 5.0 |
| FC ($d < 0.075$ mm) (%) | 11 |

Maximum and minimum void ratios have been evaluated according to ASTM [4] Method A and ASTM [3] Method 1A, respectively

cell pressure (Fig. 3b), which may be controlled independently by the vertical stress.

The configuration with flexible boundaries (Fig. 3b) imposes a constant diameter during the consolidation, simulating a "$K_0$ *condition*", which is possible through a sophisticated control system. Known the volume change and the vertical settlement of the specimen, the vertical load is adjusted to keep the diameter constant. However, the closed-loop control needed to impose the constant diameter introduces unavoidable oscillations of the radial strain around 0. In other words, a true $K_0$ condition (radial strain $\varepsilon_r = 0$) does not occur. Indeed, Okochi and Tatsuoka [27] have shown that a radial strain of around $10^{-2}$% may induce an error of 5% in $K_0$ estimation. In Sect. 3.1, radial strains and the error induced in $K_0$ estimation will be quantified.

During the shear loading, the feedback system allows keeping the total vertical stress constant, changing the cell pressure. An active height control keeps the height of the specimen constant (e.g. vertical strains are lower than ± 0.05%, ASTM [5, 6]). Since the height and volume are both constant (undrained tests), the cross-sectional area does not change, as well. During the undrained shearing phase, the excess pore pressure may be measured by means of a pore pressure transducer, while vertical and horizontal displacements can be measured by using vertical and horizontal LVDTs.

The shear loading is applied at the bottom of the specimen. Since no complementary shear stress exists on the vertical boundary planes, the distribution of horizontal shear stresses on top and bottom is not uniform. It implies that the vertical stress distribution on top and bottom is also not uniform owing to the need to preserve moment equilibrium. Nevertheless, the tests have been interpreted considering the horizontal shear stress ($\tau$) as the average shear stress in horizontal direction and assuming the

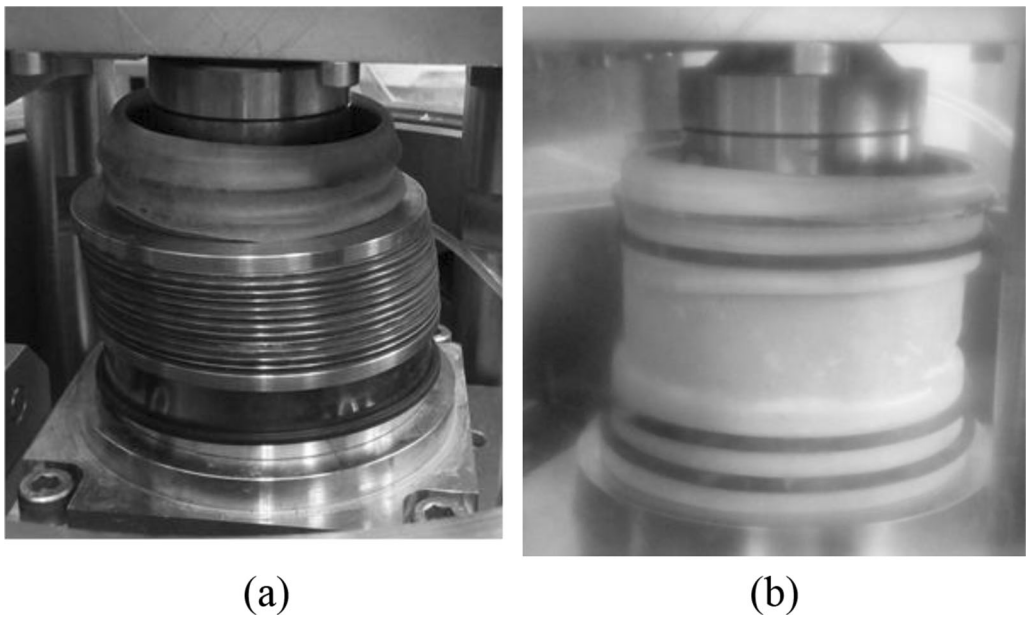


**Fig. 3** SS soil specimen enclosed with rigid rings (**a**) and unreinforced latex membrane (**b**)

complementary shear stress on vertical planes of the specimens. This simplification, even though not totally accurate, has allowed to interpret the results in the plane $p'-q$ as also reported by Mao and Fahey [21].

In this research, only the results performed on specimens enclosed with unreinforced membrane are shown. These tests will be simply referred to as *simple shear* tests to make a clear distinction from *direct simple shear* tests, where rigid boundaries confined the specimens [10]. The apparatus is shown in Fig. 4.

## 3 Experimental activity

Eleven monotonic and four cyclic simple shear tests have been performed. The specimens have been prepared by moist tamping technique in order to investigate a wide range of relative densities ($20 \leq D_r$ (%) $\leq 76$). In moist tamping technique, dry sand is initially mixed with water that represents 5% water content of the specimen. Then, the moist sand is compacted into two layers inside a split mould. Each layer is compacted into a designated portion of the required dry unit weight of the specimen. Specimens have been saturated by increasing the back pressure until $B$-value $\geq 0.95$ is achieved. The saturation of sandy specimens takes about 20 h. After that, the specimens have been consolidated at different confining stresses ($\sigma'_h$), with vertical effective stresses ($\sigma'_v$) ranging between 49 and 206 kPa (Tab. 2).

After consolidation, the specimens have been subjected to shear phases. The monotonic tests have been carried out in strain-controlled mode, imposing a displacement rate of 0.03 mm/min. On the contrary, cyclic tests have been performed in stress-controlled mode by applying sinusoidal shape of loading with a frequency of 0.05 Hz and different cyclic stress ratios (CSR = $\tau/\sigma'_v$).

### 3.1 "$K_0$ consolidation" in simple shear tests with confining pressure

The control system needed to impose simple shear conditions introduces unavoidable oscillations of the diameter's measure around the target value. Quantifying these oscillations is extremely important to understand if truly simple shear conditions occur. In other words, to avoid the onset of plastic deformations, which would change the diameter permanently [20], the radial strains ($\varepsilon_r$) should be small enough to remain in elastic region. In this framework, the radial strains have been computed during the "$K_0$-consolidation" phase. As an example, in Fig. 5 $\varepsilon_r$ is plotted versus time for a loose (SS_GSS3; a) and a dense (SS_GSS5; b) specimen (Table 2).

In both cases, the radial strains have an order of magnitude of $10^{-3}$% that can be considered low enough to assume the deformations belong to the elastic region (the elastic threshold is generally indicated with the value of $10^{-3}$%).

However, as a further confirmation of the reliability of experimental data, the ratio between $\sigma'_h$ and $\sigma'_v$, called $K^*$ in this paper to distinguish it from $K_0$ ($\varepsilon_r = 0$), has been compared with the coefficient of earth pressure at rest ($K_0$). Lirer et al. [20] proposed an estimation of $K_0$ introducing

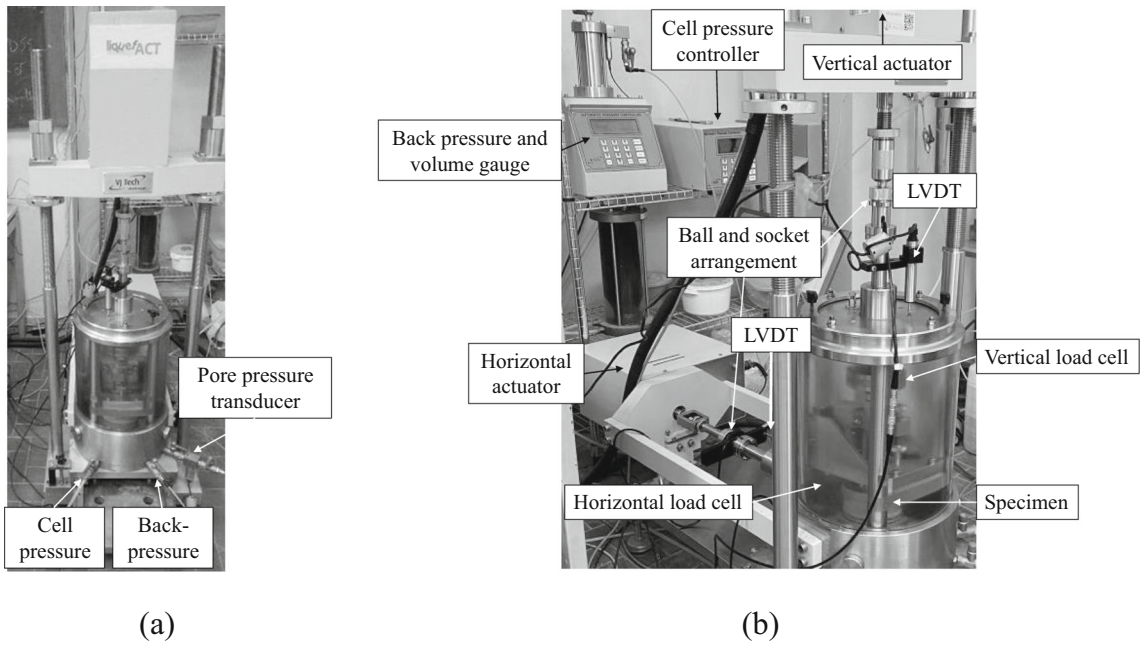


**Fig. 4** Simple shear device at University of Napoli Federico II: frontal (**a**) and lateral (**b**) view

**Table 2** Testing program of SS tests on Pieve di Cento sand

| Test | Kind of test | *B* values | *e** | Dr* (%) | $\sigma'_h$ (kPa) | $\sigma'_v$ (kPa) | CSR |
|---|---|---|---|---|---|---|---|
| SS_GSS1 | Monotonic | 0.97 | 0.793 | 21 | 28.3 | 53.5 | – |
| SS_GSS2 | | 0.97 | 0.754 | 29 | 20.0 | 49.2 | – |
| SS_GSS3 | | 0.96 | 0.689 | 44 | 21.4 | 49.1 | – |
| SS_GSS4 | | 0.95 | 0.668 | 49 | 22.2 | 49.4 | – |
| SS_GSS5 | | 0.95 | 0.602 | 64 | 22.2 | 53.6 | – |
| SS_GSS6 | | 0.96 | 0.581 | 68 | 17.3 | 60.1 | – |
| SS_GSS7 | | 0.95 | 0.690 | 44 | 45.2 | 94.2 | – |
| SS_GSS8 | | 0.95 | 0.660 | 51 | 39.8 | 109.3 | – |
| SS_GSS9 | | 0.95 | 0.549 | 76 | 35.3 | 99.4 | – |
| SS_GSS10 | | 0.98 | 0.655 | 52 | 83.1 | 206.5 | – |
| SS_GSS11 | | 0.96 | 0.537 | 78 | 96.5 | 194.1 | – |
| CSS_GSS1 | Cyclic | 0.95 | 0.683 | 45 | 25.7 | 53.1 | 0.130 |
| CSS_GSS2 | | 0.95 | 0.699 | 42 | 26.6 | 52.3 | 0.136 |
| CSS_GSS3 | | 0.97 | 0.710 | 39 | 23.7 | 49.5 | 0.132 |
| CSS_GSS4 | | 0.97 | 0.702 | 41 | 28.6 | 57.2 | 0.110 |

*After consolidation phase

some hypotheses within a simple elastoplastic constitutive framework. It is given by:

$$K_0 = \frac{[(3-2\cdot M)\cdot(\varsigma-1)+3\cdot(\varsigma+2)]\cdot K^* + (3-M)\cdot(\varsigma-1)}{2\cdot(\varsigma-1)\cdot(3+2\cdot M)\cdot k^* + (3+2\cdot M)\cdot(\varsigma-1)+9} \quad (7)$$

where $M$ is a material constant and $\varsigma$ is a parameter that depends on the ratio between total radial ($\dot{\varepsilon}_r$) and axial strain ($\dot{\varepsilon}_a$) increments:

$$\varsigma = \frac{1+2\cdot\frac{\dot{\varepsilon}_r}{\dot{\varepsilon}_a}}{1-\frac{\dot{\varepsilon}_r}{\dot{\varepsilon}_a}} \quad (8)$$

In Table 3, the values of $K^*$ computed at the end of consolidation are compared with the theoretical values of $K_0$ (Eq. 7) for each simple shear test (assuming $M$ = 1.35 as reported by Flora et al. [14]). Apart from SS_GSS11 and CSS_GSS2 tests, where the difference between $K^*$ and $K_0$ is relevant (the error is 9.89% and 9.10%, respectively, see Table 3), the values of $K^*$ and $K_0$ are mostly very similar. The error is generally lower than 6%.

Since the radial strains induced by the control system are not relevant (Fig. 5), the difference between the experimentally determined values of $K^*$ and $K_0$ is very small. It confirms the reliability of the control system and thus a good approximation of simple shear conditions.

## 3.2 Undrained monotonic tests

As an example, Fig. 6 shows the results of three monotonic tests (SS_GSS2; SS_GSS4; SS_GSS5 in the following planes: $\gamma-\tau$ (a), $\gamma-\Delta u$ (b) and $\sigma'_v - \tau$ (c).

As expected, the denser specimen (SS_GSS5) exhibits a clear strain hardening-type response (Fig. 6a) with higher negative excess pore water pressure than looser specimens. However, all of them exhibit a dilatative behaviour. It suggests that the initial state of all specimens is below the

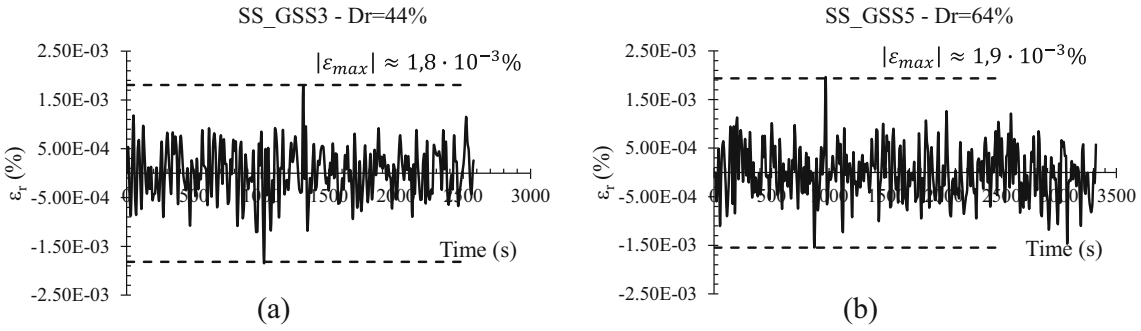


**Fig. 5** Radial strains with time during $K_0$ consolidation for a loose (**a**) and a dense specimen (**b**)

**Table 3** Comparisons between $K^*$ and $K_0$

| Test | Kind of test | Dr (%) | $\sigma'_h$ (kPa) | $\sigma'_v$ (kPa) | $K^*$ | $K_0$ Eq. (7) | \|Error\| (%) |
|---|---|---|---|---|---|---|---|
| SS_GSS1 | Monotonic | 21 | 28.3 | 53.5 | 0.530 | 0.549 | 3.39 |
| SS_GSS2 | | 29 | 20.0 | 49.2 | 0.406 | 0.412 | 1.42 |
| SS_GSS3 | | 44 | 21.4 | 49.1 | 0.436 | 0.432 | 0.91 |
| SS_GSS4 | | 49 | 22.2 | 49.4 | 0.449 | 0.471 | 4.75 |
| SS_GSS5 | | 64 | 22.2 | 53.6 | 0.414 | 0.409 | 1.12 |
| SS_GSS6 | | 68 | 17.3 | 60.1 | 0.287 | 0.287 | 0.05 |
| SS_GSS7 | | 44 | 45.2 | 94.2 | 0.436 | 0.432 | 0.91 |
| SS_GSS8 | | 51 | 39.8 | 109.3 | 0.364 | 0.366 | 0.30 |
| SS_GSS9 | | 76 | 35.3 | 99.4 | 0.355 | 0.356 | 0.26 |
| SS_GSS10 | | 52 | 83.1 | 206.5 | 0.403 | 0.426 | 5.42 |
| SS_GSS11 | | 78 | 96.5 | 194.1 | 0.497 | 0.552 | 9.89 |
| CSS_GSS1 | Cyclic | 45 | 25.7 | 53.1 | 0.483 | 0.515 | 6.16 |
| CSS_GSS2 | | 42 | 26.6 | 52.3 | 0.506 | 0.485 | 9.10 |
| CSS_GSS3 | | 39 | 23.7 | 49.5 | 0.479 | 0.489 | 2.03 |
| CSS_GSS4 | | 41 | 28.6 | 57.2 | 0.499 | 0.490 | 1.98 |

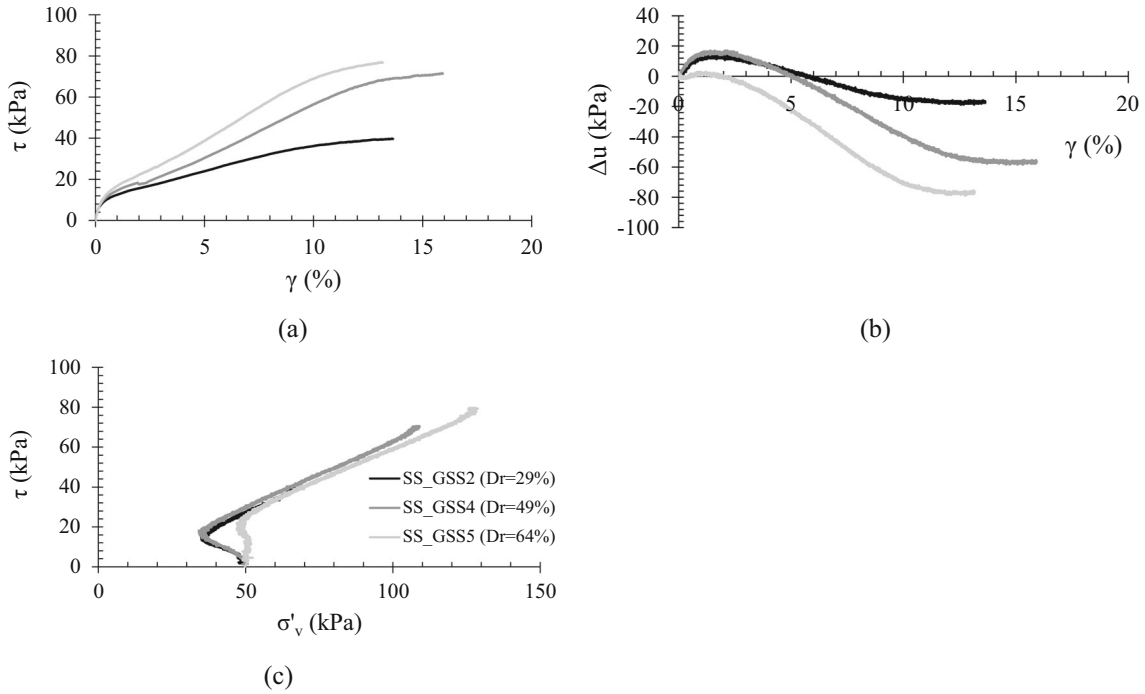


**Fig. 6** Results of monotonic triaxial tests in the planes $\gamma - \tau$ (**a**), $\gamma - \Delta u$ (**b**) and $\sigma'_v - \tau$ (**c**)

critical state line (CSL in $p'-e$ plane). Moreover, it is worth noting that all of them have reached the critical state conditions (no further change of $\Delta u$).

### 3.2.1 Interpretation of monotonic tests

As already mentioned in the first part of the paper, the interpretation of simple shear tests is not universally agreed upon and this topic is still widely being discussed today in literatures. However, based on the aforementioned simplifications (complementary of shear stress, uniformity of stress state, horizontal stress equal to cell pressure) the principal normal effective stresses ($\sigma'_1$, $\sigma'_2$, $\sigma'_3$) can be obtained via Eq. (1).

The results of SS_GSS2, SS_GSS4 and SS_GSS5 tests have been plotted in the principal stress space $\sigma'_1-\sigma'_2-\sigma'_3$

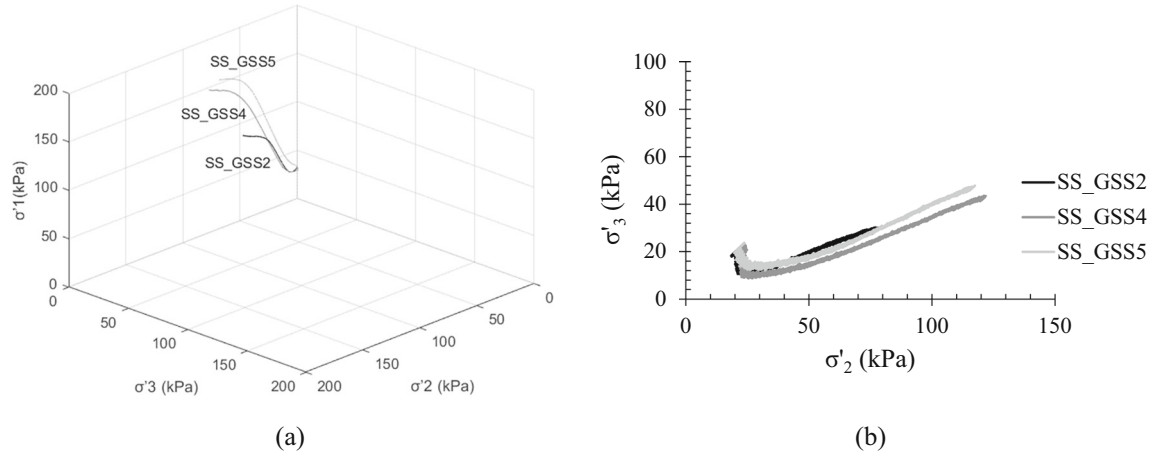


**Fig. 7** Stress path of SS_GSS2, SS_GSS4 and SS_GSS5 tests in principal stress space (**a**) and in $\sigma'_2 - \sigma'_3$ plane (**b**)

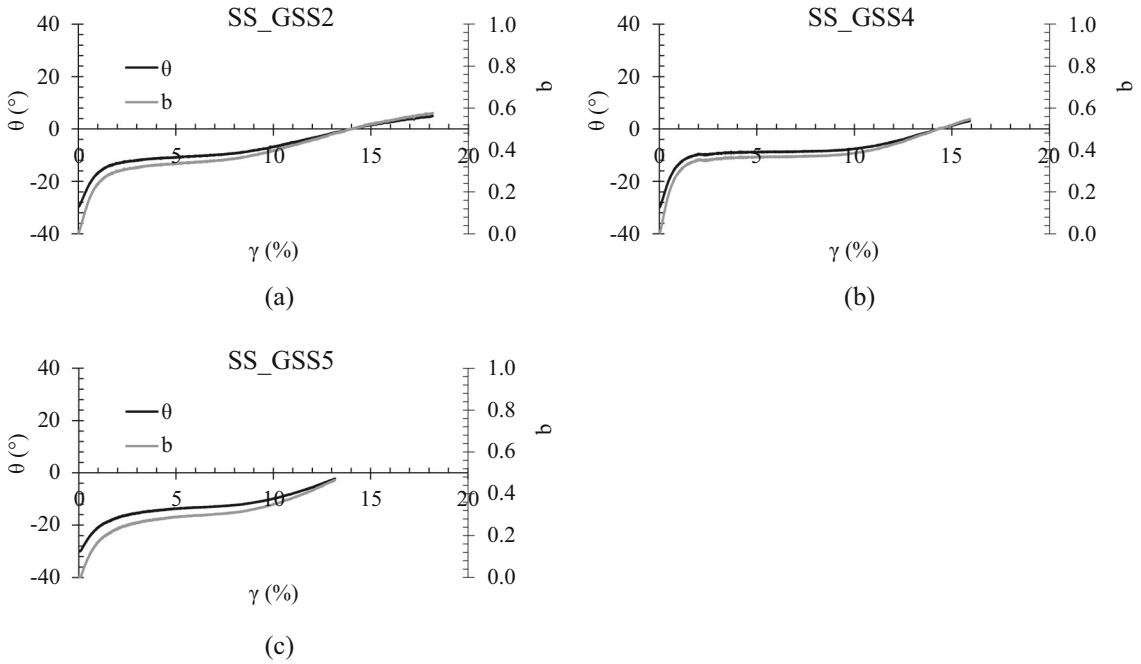


**Fig. 8** $b$ and $\theta$ with $\gamma$ for SS_GSS2 (**a**), SS_GSS4 (**b**) and SS_GSS5 (**c**) tests

(Fig. 7a). At the beginning of deviatoric phase, we have $\sigma'_2 = \sigma'_3 \neq \sigma'_1$. During the progression of the test, $\sigma'_2$ grows faster than $\sigma'_3$ and the stress path moves towards the left (Fig. 7b). This trend is in agreement with the theoretical trend shown by Doherty and Fahey [13].

Known the intermediate effective stress ($\sigma'_2 = \sigma'_h$), Lode's angle ($\theta$) and the intermediate principal stress coefficient (b) may be evaluated via Eqs. (4, 5), respectively. As an example, $\theta$ and $b$ of SS_GSS2, SS_GSS4 and SS_GSS5 tests are plotted in Fig. 8 with the shear strain ($\gamma$).

Lode's angle starts from $-30°$ and increases intercepting 0 when $\gamma$ is about 15%. On the other hand, $b$ starts from 0 and when $\theta$ is 0, $b$ is 0.5. This means that the effective intermediate principal stress ($\sigma'_2$) is midway between the major ($\sigma'_1$) and minor ($\sigma'_3$) principal effective stresses. The experimental results show that $\theta = 0$ (hence $b = 0.5$) is attained when the critical state condition is reached.

Given that a reasonable estimation was achieved, the complete stress state within the specimen has been made, and the Mohr's circles can be plotted. As an example, in Fig. 9a, c and e the Mohr's circles at the initial and final conditions are depicted, for SS_GSS2, SS_GSS4 and SS_GSS5 tests, respectively.

At the beginning of the shear phase ($\tau = 0$), the pole of the circle is coincident with the horizontal stress, which is

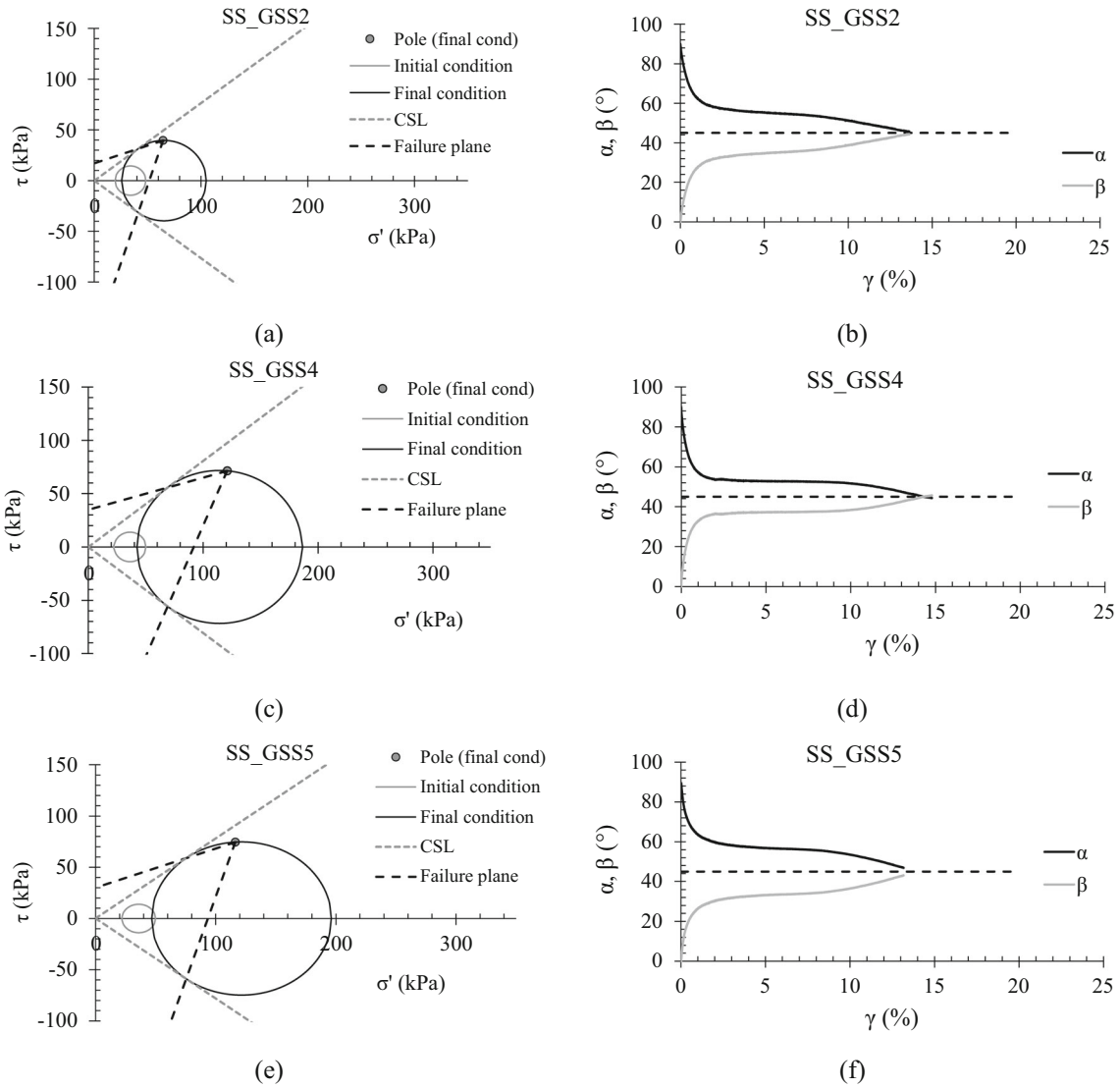


**Fig. 9** Interpretation of undrained simple shear tests by means of Mohr's circle for several tests (**a**, **c**, **e**) and rotation of principal stress directions with $\gamma$ (**b**, **d**, **f**), where $\alpha$ and $\beta$ are the inclinations of major ($\sigma'_1$) and minor ($\sigma'_3$) principal stress directions, respectively

the minimum principal stress ($\sigma'_h = \sigma'_3$). Indeed, the vertical and horizontal principal stress directions are inclined at 90° ($\alpha$) and 0° ($\beta$) from horizontal, respectively.

As the shear stress increases, the pole moves on the Mohr's circle and $\alpha$ decreases—on the contrary, $\beta$ increases (rotating in the opposite direction)—until reaching a value of 45° (Fig. 9b, d, f) when failure occurs. In other words, the pole tends to reach the top of the Mohr's circle, meaning that the horizontal plane is the plane of maximum shear stress at large strains, as stated by the theory of Roscoe [31]. However, the stress state on the horizontal plane does not represent the worst failure condition for the soil element. The slope of the failure envelope, which touches the Mohr's circle, is about 38° (Fig. 9a, c, e).

The failure condition may be prescribed by the stress state associated with an inclined plane. The failure plane, obtained by connecting the pole with the point of tangency, is inclined at 19° counterclockwise to the horizontal plane (Fig. 9a, c, e) (for positive shear stresses). This is in agreement with the experimental results proposed by Budhu [9] and the theoretical ones reported by Doherty and Fahey [13]. Budhu [9] showed that the angle to the

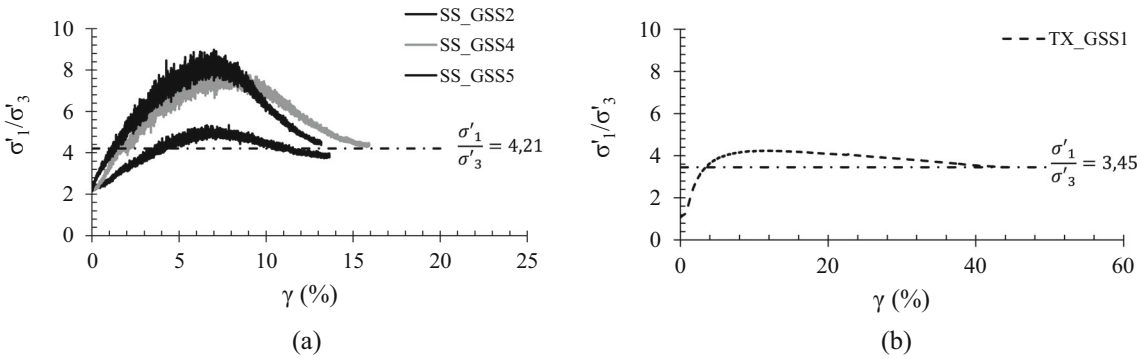


**Fig. 10** Comparison between the results of simple shear (**a**) and triaxial (**b**) tests in the plane $\gamma - \sigma'_1/\sigma'_3$

horizontal planes of the rupture surface is about 14°, while Doherty and Fahey [13], who performed FEM analyses, found that the maximum friction angle occurs on a plane at 16° to the horizontal.

### 3.2.2 Comparisons with triaxial tests and critical state condition

In order to compare the results of simple shear tests with those carried out with triaxial apparatus, the experimental data have been interpreted in the plane $\gamma - \sigma'_1/\sigma'_3$. In Fig. 10, the results of SS_GSS2, SS_GSS4 and SS_GSS5 simple shear tests (Fig. 10a) are compared with that of an undrained triaxial test (Fig. 10b) performed on the same sand by Flora et al. [14] (TX_GSS1 test: $D_r = 51\%$, $\sigma'_{c} = 50$ kPa). It should be specified that the axial strains of triaxial test have been converted in shear strains ($\gamma = 1.5 \cdot \varepsilon_a$) to correlate the testing data.

Since TX_GSS1 test is consolidated under isotropic condition ($\sigma'_1 = \sigma'_3$), the path starts from $\sigma'_1/\sigma'_3 = 1$, while the initial value of the ratio $\sigma'_1/\sigma'_3$ is about 2 for simple shear tests. However, both triaxial and simple shear tests reach a stationary value of the ratio $\sigma'_1/\sigma'_3$. It is about 4.21 for SS tests (Fig. 10a) and 3.45 for TX test (Fig. 10b). Known that $\sigma'_1/\sigma'_3 = (1 + \sin\varphi')/(1 - \sin\varphi')$, the friction angle may be estimated for SS and TX tests ($\varphi' = 38°$ for simple shear tests and $\varphi' = 33°$ for triaxial test). As stated by Lanier [17], since no rotation of principal stress direction occurs in triaxial device, the friction angle is generally underestimated in these tests compared to that achieved in simple shear tests.

Further considerations have been done interpreting the results in terms of $p'-q$. In Fig. 11a, the results of SS_GSS2, SS_GSS4 and SS_GSS5 simple shear tests are plotted in the plane $p'-q$, where the two invariants have been obtained via Eqs. (2, 3), respectively. Although the stress paths of the simple shear tests start from the same stress conditions ($p''_0 \approx 30$ kPa and $q_0 \approx 25$ kPa), they exhibit different behaviours, due to the different relative densities (Table 3). In Fig. 11b, the same simple shear tests are plotted together with the stress path of TX_GSS1 test. TX_GSS1 test exhibits higher deviatoric and mean effective stresses compared to those of simple shear tests. Once again, the difference may be related to the rotation of the principal stress directions, which does not occur in triaxial test. In triaxial tests, the third invariant ($b$ or $\theta$) is constant. On the contrary, it varies in simple shear tests. When the stationary condition (critical state) is reached, $b$ and $\theta$ are 0.5 and 0°, respectively (Fig. 8).

The friction angle in critical state conditions ($\varphi'_{cv}$) may be computed by Eq. (6), assuming $\theta = -30°$ in triaxial tests and $\theta = 0°$ in simple shear tests. It results 38° for SS

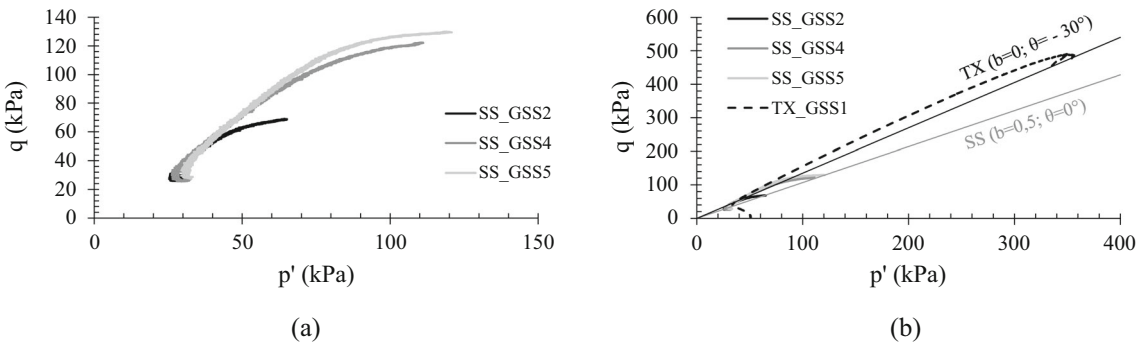


**Fig. 11** Results of simple shear tests (**a**) and comparison with compression triaxial (**b**) test in the plane $p' - q$

tests and 33° for TX test, confirming the values obtained by interpreting the results in the plane $\gamma-\sigma'_1/\sigma'_3$ (Fig. 10) and those obtained by interpreting the results with Mohr's circles (Fig. 9a, c, e). It is worth noting that even though the ratio $q/p'$ is higher in TX tests, $\varphi'_{cv}$ is lower than that evaluated in SS tests. It is due to the fact that the friction angle does depend not only on the value of $q/p'$ but also on $\theta$, as clearly stated by Eq. (6).

Even though the tests shown in Fig. 6 reach the critical state condition, some tests of the dataset do not reach the stationary conditions for shear strains of 15 or 20%. Therefore, an extrapolation process is needed to study the critical state condition of GSS sand. The approach of Murthy et al. [26] has been used, adapting it to the results of SS tests. Further details are reported in Appendix. It is worth noting that all the results of SS tests—reported in Table 3—confirm the findings shown in Figs. 10 and 11, even though they are not reported for the sake of brevity.

Moreover, further efforts have been done to identify the critical state line (CSL) in the plane $p'-e$. In Fig. 12, the CSL—represented by a power function according to Li and Wang [18]—is plotted to fit the experimental data. The equation is shown in Fig. 12.

## 3.3 Undrained cyclic tests

It is well known that liquefaction is a phenomenon which occurs in saturated sandy soil deposits subjected to earthquake shaking or other forms of rapid loading. Under these conditions, when the effective stresses approach zero, soil behaviour switches from that of a solid state to that of a fluid [19, 22]. Undrained cyclic simple shear tests allow to investigate the liquefaction behaviour of sandy soils. In laboratory, the attainment of liquefaction is generally identified with stress ($r_u = 0.90$ for silty sand, where $r_u$ is the excess pore pressure ratio, given by $\Delta u/\sigma'_v$) or strain criteria ($\gamma_{SA} = 3.75\%$, where $\gamma_{SA}$ is the shear strain in single amplitude) [15]. In this section, the results of cyclic simple shear tests on GSS have been presented.

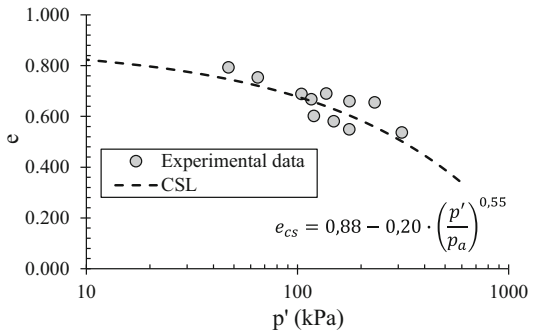


**Fig. 12** Critical state line of Pieve di Cento sand

As an example, in Fig. 13 the results of CSS_GSS1 cyclic test are reported in the following planes: γ-τ (a); $N_{cyc}-r_u-\gamma$ (b); σ′−τ (c) and $N_{cyc}-\sigma'$ (d), where $N_{cyc}$ is the applied number of constant amplitude stress cycles.

Obviously, during the shaking phase, the area of cycle in the plane $\tau-\gamma$ increases (Fig. 13a). The excess pore pressure ratio ($r_u$) increases until reaching liquefaction ($r_u = 0.90$) after nine cycles, while $\gamma$ does not exceed a value of 4% in double amplitude (Fig. 13b). In Fig. 13c, the stress path is plotted. During the cycles, the stress paths move to the origin of the axes until touching the failure envelope, which is consistent with the static characterization of GSS sand described in the previous paragraph. In Fig. 13d, due to the pore pressure build-up, the effective—vertical and horizontal—stresses decrease with $N_{cyc}$. $\sigma'_v$ decreases faster than $\sigma'_h$ and when liquefaction occurs ($r_u = 0.90$), $\sigma'_v$ and $\sigma'_h$ tend to assume the same values (isotropic condition).

### 3.3.1 Interpretation of cyclic tests

Based on the same simplifications adopted to interpret the results of monotonic tests, Mohr's circles may be represented for cyclic undrained simple shear tests, as well.

At the beginning of the shearing phase (indicated as $N_{cyc} = 0$ in Fig. 14a) and at every half cycle, when $\tau$ is equal to 0 in sinusoidal waveform, vertical ($\sigma'_v$) and horizontal ($\sigma'_h$) stresses are principal stress directions. Their difference (the diameter of Mohr's circle) decreases during the test (Fig. 14a), until reaching an isotropic state ($K^* \approx 1$), where the Mohr's circle collapses to a single point.

The principal stress directions can be identified from the pole of Mohr's circle, which moves along the circumference during the tests. The inclination of the major ($\sigma'_1$) and minor principal stresses ($\sigma'_3$)—α and $\beta$, respectively—can be plotted with $N_{cyc}$ and is reported in Fig. 14b. It is worth noting that α and β have been computed when the imposed sinusoidal shear stress is maximum ($\tau = \tau_{max}$) in each loading cycle.

Obviously, at the beginning of cyclic loading the major ($\sigma'_1$) and minor principal stress ($\sigma'_3$) directions are inclined of 90° and 0°, respectively. During the cycles, α decreases, while $\beta$ increases until attaining an asymptotic value of 45°.

Liquefaction is attained when $\alpha = \beta = 45°$, such a value is critical as indicated by Sivathayalan et al. [32]. According to them, under these conditions the alignment of the plane of maximum shear stress with the bedding plane of specimens prepared by water pluviation technique occurs. However, the critical value of 45° seems to be true also in moist tamped specimens (this study) where a "honeycomb structure" is likely formed [33]. Even though a bedding plane could not be clearly formed with moist

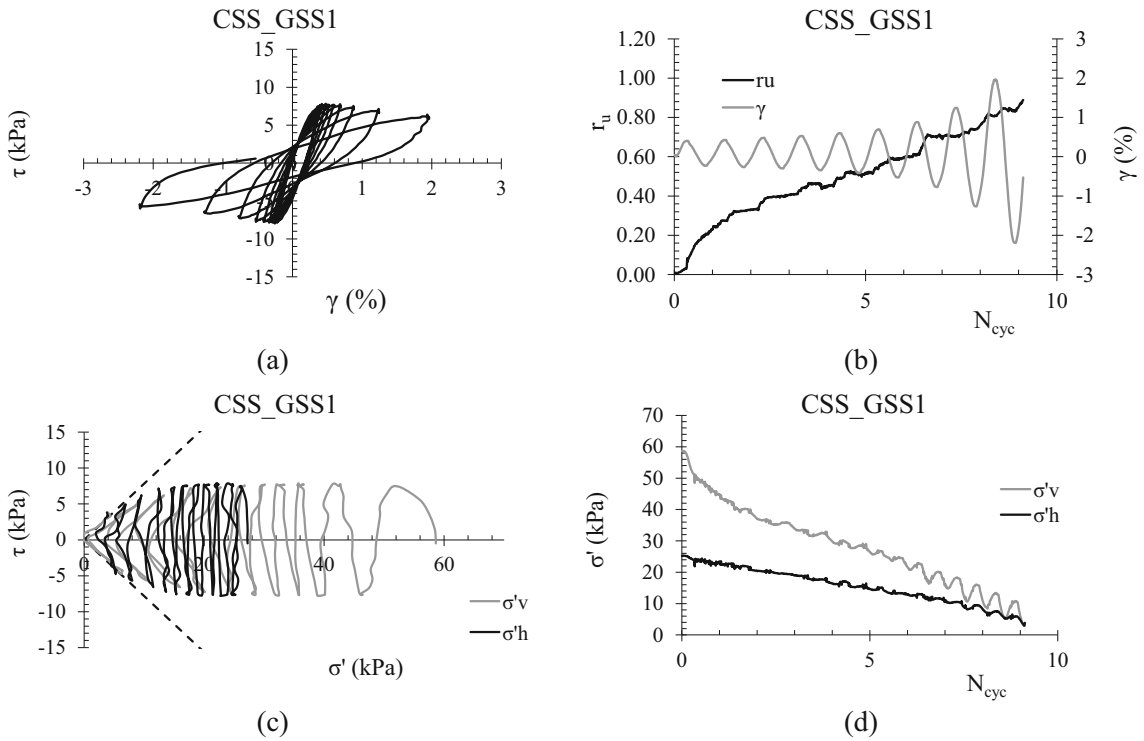


**Fig. 13** Results of CSS_GSS1 cyclic test in the planes: $\gamma - \tau$ (**a**); $N_{cyc} - r_u - \gamma$ (**b**); $\sigma' - \tau$ (**c**); $N_{cyc} - \sigma'$ (d)

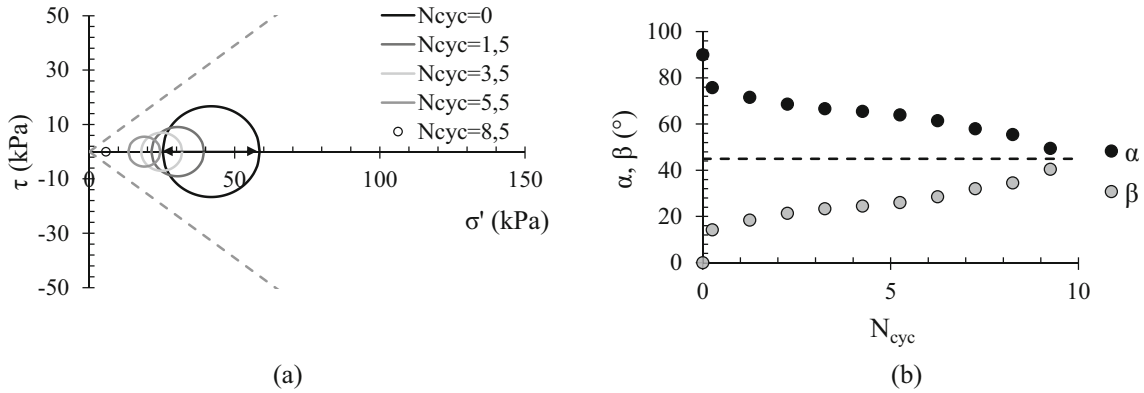


**Fig. 14** CSS_GSS1 test: Mohr's circles for $\tau = 0$ (**a**) and rotation of principal stress directions for $\tau = \tau_{max}$ (one quarter of each sinusoidal loading cycle) (**b**), where $\alpha$ and $\beta$ are the inclinations of major ($\sigma'_1$) and minor ($\sigma'_3$) principal stress directions, respectively

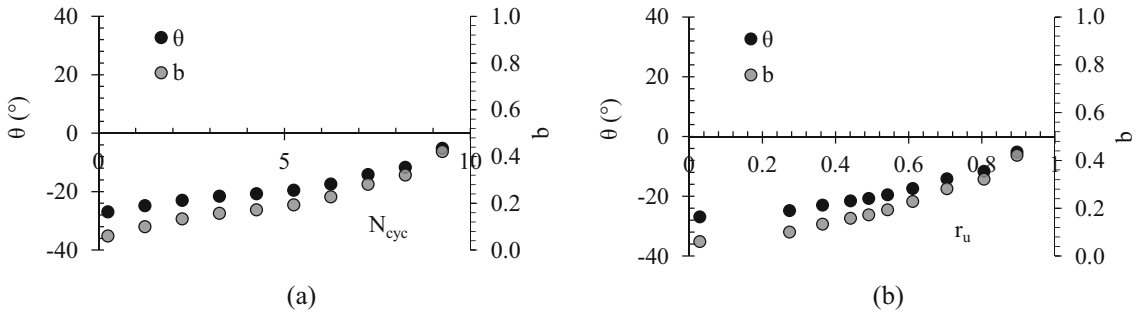


**Fig. 15** CSS_GSS1 test: $b$ and $\theta$ versus $N_{cyc}$ (**a**) and $r_u$ (b)

tamping technique, weaker horizontal zones could be generated in correspondence to the separation layers.

The role of $\theta$ and $b$ in cyclic simple shear tests has been examined. In Fig. 15a, $\theta$ and $b$ are plotted with $N_{cyc}$ for each one quarter of sinusoidal loading cycle ($\tau = \tau_{max}$) for CSS_GSS1 test. As expected, $\theta$ starts from $-30°$ and decreases with $N_{cyc}$, until intercepting 0 after nine cycles (liquefaction triggering). On the other hand, $b$ starts from 0 and when liquefaction occurs it is about 0.5. It is much more evident by plotting $\theta$ and $b$ with $r_u$ (Fig. 15b). When $r_u = 0.90$, $\theta$ and $b$ are 0 and 0.5, respectively.

The results show that liquefaction triggers when the effective intermediate principal stress is midway between the major and minor principal effective stresses ($b = 0.5$ and consequently $\theta = 0$).

### 3.3.2 Cyclic resistance curve and comparisons with cyclic triaxial tests

The results of undrained cyclic tests on sandy soils are usually interpreted in the CRR–$N_{liq}$ plane. $N_{liq}$ is the value of $N_{cyc}$ needed to reach liquefaction for a given value of CSR. For $N_{cyc} = N_{liq}$, the applied cyclic stress ratio represents the cyclic resistance ratio (or CRR). The locus ($N_{liq}$ - CRR) identifies the cyclic resistance curve. The results of cyclic simple shear tests have been reported in the plane $N_{liq}$–CRR, where $N_{liq}$ has been identified according to the stress criterion ($r_u = 0.90$).

In order to compare the results of cyclic triaxial (CTX) and simple shear (CSS) tests, the correlation proposed by Castro [11] may be used. Castro [11] proposed a correction factor ($c_r$) to take into account the effects of different stress paths. According to him, CRR in cyclic triaxial tests ($CRR_{ctx}$) and CRR in cyclic simple shear tests ($CRR_{css}$) are linked through the following equation:

$$CRR_{css} = c_r \cdot CRR_{ctx} \tag{9}$$

The correction factor ($c_r$) is a function of the coefficient of earth pressure at rest, $K_0$, according to the following equation:

$$c_r = \frac{2 \cdot (1 + 2 \cdot K_0)}{3\sqrt{3}} \tag{10}$$

To compare the results of CSS and CTX (published by Mele et al., [25]) tests, the values of $CSR_{ctx}$ have been transformed in $CRR_{css}$ via Eq. (9). It was assumed $K_0 = K^*$, where $K^*$ has been evaluated experimentally as the ratio between $\sigma'_h$ and $\sigma'_v$ and is reported in Table 3. The average value of $K^*$ (0.490) is used in Eq. (10) to estimate $c_r$ (0.764). Figure 16 shows that the experimental data points from CTX tests fit those of CSS tests, confirming, once again, the reliability of the tests and the measures of $K^*$, which well approximates $K_0$ ($\varepsilon_r = 0$).

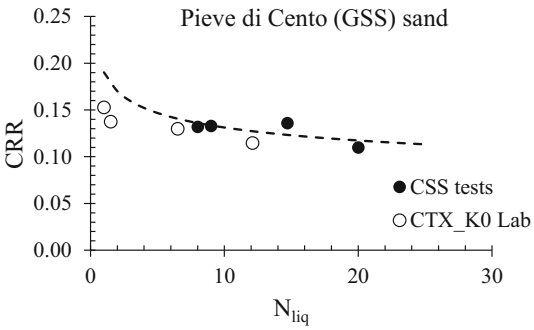


**Fig. 16** Comparison between CTX ($D_r \approx 40\%$ and $\sigma''_c = 50$ kPa) and CSS tests in the plane $N_{liq}$–CRR by using $K^*$ estimated from laboratory tests

## 4 Conclusions

In this paper, the results of undrained monotonic and cyclic simple shear tests performed with flexible boundaries have been presented and discussed. The apparatus is able to reproduce a "$K_0$ condition" through a sophisticated control system, whose accuracy has been carefully examined and discussed. The unavoidable oscillations of the diameter's measure around the target value have been quantified. They may be considered low enough to consider a truly simple shear condition, as confirmed by the small difference between the experimentally determined value of $K^*$ and $K_0$ (computed within a simple elastoplastic constitutive framework). The results of undrained monotonic and cyclic simple shear tests have been interpreted under the hypotheses of uniformity of stress state and complementarity of shear stresses on the vertical planes of the specimen. This has allowed for the plotting Mohr's circles and to give a reasonable estimation of the complete stress state within the specimen. The main results are summarized as follows:

- Soil failure under monotonic and cyclic loading is reached when the effective intermediate principal stress ($\sigma'_2$) is midway between the major ($\sigma'_1$) and minor ($\sigma'_3$) principal effective stresses ($b = 0.5$ and $\theta = 0$), while the major and minor principal stress directions tend to reach a slope of 45°.
- The horizontal plane is the plane of maximum shear stress at large strains, confirming the theory of Roscoe [26].
- The failure plane is generally inclined at 19° counterclockwise to the horizontal plane, in agreement with the experimental and numerical results reported by other authors.
- Pieve di Cento sand's friction angle resulting from simple shear tests is higher ($\varphi'_{cv} = 38°$) than that obtained in triaxial tests ($\varphi'_{cv} = 33°$) which are performed in b-constant condition.

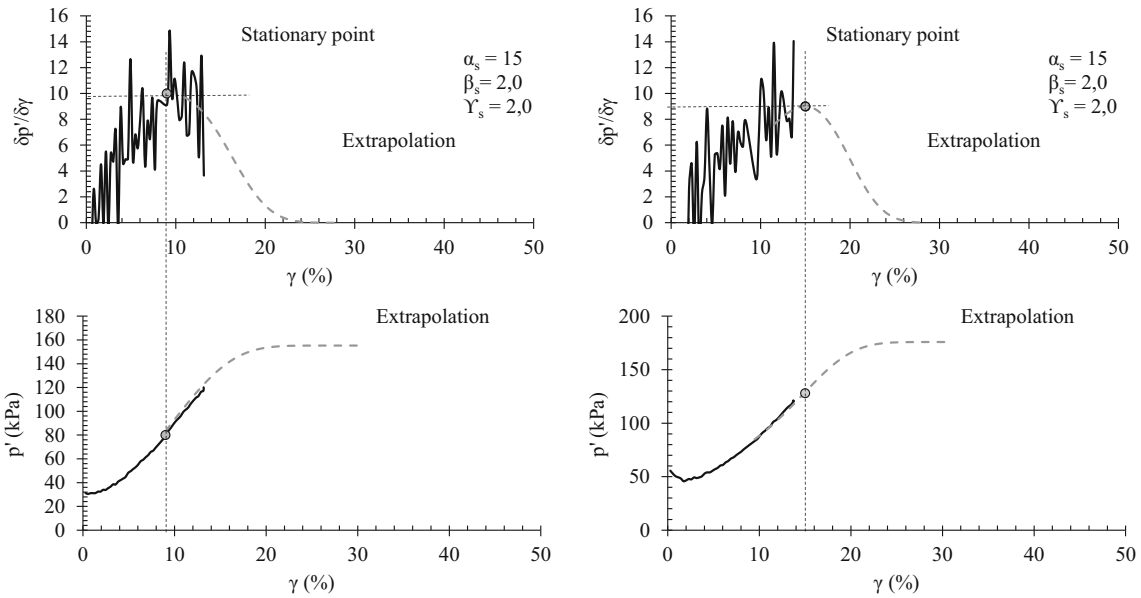


**Fig. 17** Extrapolation procedure for SS_GSS5 (**a**) and SS_GSS9 (**b**) tests to find the critical state condition

- In undrained cyclic tests, the stress state tends to an isotropic condition ($K^* \approx 1$), due to the change of state of the soil from solid to fluid.
- The cyclic resistance curve achieved from cyclic triaxial tests is in agreement with that observed in simple shear tests ($CRR_{15} \approx 0.13$), adopting the $K_0$ (or $K^*$) evaluated from laboratory tests.

## Appendix

### Extrapolation procedures to evaluate the critical state of sands

Murthy et al. [26] proposed an extrapolation procedure to evaluate the critical state of sands in undrained triaxial tests. According to it, the critical state may be evaluated through the best fitting of sigmoidal function on the curve of $\partial p'/\partial \varepsilon_a$ versus $\varepsilon_a$ with the experimental results.

The mathematical expression of the sigmoidal function is reported as follows:

$$\frac{\partial p'}{\partial \varepsilon_a} = \left(\frac{\partial p'}{\partial \varepsilon_a}\right)_0 \cdot \exp\left(-\left\{\left[\left(\frac{\varepsilon_a}{\alpha_s}\right)^{\gamma_s} - \left(\frac{\varepsilon_{1,0}}{\alpha_s}\right)^{\gamma_s}\right]^{\beta_s}\right\}\right) \quad (11)$$

where $\alpha_s$, $\beta_s$ and $\gamma_s$ are fitting parameters, while $\varepsilon_{1,0}$ and $\left(\frac{\partial p'}{\partial \varepsilon_a}\right)_0$ are the axial strain and the value of the first derivative of the $p'-\varepsilon_a$ curve, respectively, at the point of inflexion, which corresponds to a stationary point in the plane $\varepsilon_a - {}^{\partial p'}/_{\partial \varepsilon_a}$. From Eq. (11), it can be easily understood that the inclination of the $p'-\varepsilon_a$ curve decreases with strain and approaches zero asymptotically. The fitted response in terms of p' versus $\varepsilon_a$ can be achieved by integrating Eq. (11).

The same approach has been used in this paper for simple shear tests. In this case, $p'$ in critical state condition can be evaluated from the extrapolation of the experimental data by means of Eq. (11), replacing $\varepsilon_a$ with $\gamma$.

For greater clarity, the sigmoidal function for simple shear tests has been reported as follows:

$$\frac{\partial p'}{\partial \gamma} = \left(\frac{\partial p'}{\partial \gamma}\right)_0 \cdot \exp\left(-\left\{\left[\left(\frac{\gamma}{\alpha_s}\right)^{\gamma_s} - \left(\frac{\gamma_{1,0}}{\alpha_s}\right)^{\gamma_s}\right]^{\beta_s}\right\}\right) \quad (12)$$

As an example, the extrapolation procedure applied for SS_GSS5 and SS_GSS9 is depicted in Fig. 17.

**Acknowledgements** The author deeply acknowledges Prof. Alessandro Flora (University of Napoli Federico II) and Prof. Stefania Lirer (University of Rome Guglielmo Marconi) for their valuable suggestions and discussions on tests results and interpretation. Moreover, the author is grateful to technicians of Geotechnical Laboratory of University of Napoli Federico II Mr. Alfredo Ponzo, Mr. Antonio Cammarota and Mr. Dino De Pari for their essential technical and moral support. The author would like to acknowledge the financial support of "LIQUEFACT" Project (European project Horizon 2020; grant agreement no. 700748), which has allowed to purchase the simple shear device. The author is also grateful to the anonymous reviewers for having improved the present work.

**Data availability statement** Some or all data, models, or code that support the findings of this study are available from the corresponding author upon reasonable request.

## Declarations

**Conflict of interest** Not applicable.

## References


1. Airey DW, Wood DM (1987) An evaluation of direct simple shear tests on clay. Géotechnique 37(1):25–35
2. Andresen A, Berre T, Kleven A, Lunne T (1979) Procedures used to obtain soil parameters for foundation engineering in the North Sea. Mar Georesour Geotechnol 3(3):201–266
3. ASTM D4253-06 (2006) Standard test methods for maximum index density and unit weight of soils using a vibratory table. Annual Book of ASTM Standards, ASTM International, West Conshohocken
4. ASTM D4254-06 (2006) Test methods for minimum index density and unit weight of soils and calculation of relative density. Annual Book of ASTM Standards, ASTM International, West Conshohocken
5. ASTM D6528-17 (2017) Standard test method for consolidated undrained direct simple shear testing of fine grain soils. ASTM International: West Conshohocken
6. ASTM D8296-19 (2019) Standard test method for consolidated undrained cyclic direct simple shear test under constant volume with load control or displacement control
7. Bjerrum L, Landva A (1966) Direct simple-shear tests on a Norwegian quick clay. Geotechnique 16(1):1–20
8. Budhu M (1984) Nonuniformities imposed by simple shear apparatus. Can Geotech J 21(1):125–137
9. Budhu M (1988) Failure state of a sand in simple shear. Can Geotech J 25(2):395–400
10. Carraro JAH (2017) Analysis of simple shear tests with cell pressure confinement. Geomech Geoeng 12(3):169–180
11. Castro G (1975) Liquefaction and cyclic mobility of saturated sands. J Geotech Geoenviron Eng 101(ASCE) GT6: 551–569
12. De Josselin de Jong G (1971) Discussion to session II. In: Proceedings of the roscoe memorial symposium stress-strain behaviour of soils. Cambridge, pp 29–31
13. Doherty J, Fahey M (2011) Three-dimensional finite element analysis of the direct simple shear test. Comput Geotech 38(7):917–924
14. Flora A, Bilotta E, Chiaradonna A, Lirer S, Mele L, Pingue L (2021) A field trial to test the efficiency of induced partial saturation and horizontal drains to mitigate the susceptibility of soils to liquefaction. Bull Earthq Eng 19(10):3835–3864
15. Ishihara K (1993) Liquefaction and flow failure during earthquakes. Geotechnique 43(3):351–451
16. Kjellman W (1951) Testing the shear strength of clay in Sweden. Geotechnique 2(3):225–232
17. Lanier J (1990) Recent trends in laboratory testing. In: Geomaterials: constitutive equations and modelling. CRC Press, pp 23–42
18. Li XS, Wang Y (1998) Linear representation of steady-state line for sand. J Geotech Geoenviron Eng ASCE 124(12):1215–1217
19. Lirer S, Mele L (2019) On the apparent viscosity of granular soils during liquefaction tests. Bull Earthq Eng 17(11):5809–5824
20. Lirer S, Flora A, Nicotera MV (2011) Some remarks on the coefficient of earth pressure at rest in compacted sandy gravel. Acta Geotech 6(1):1–12
21. Mao X, Fahey M (2003) Behaviour of calcareous soils in undrained cyclic simple shear. Géotechnique 53(8):715–727
22. Mele L (2022) An experimental study on the apparent viscosity of sandy soils: from liquefaction triggering to pseudo-plastic behaviour of liquefied sands. Acta Geotech. https://doi.org/10.1007/s11440-021-01261-2
23. Mele L, Lirer S, Flora A (2019a) The effect of confinement in liquefaction tests carried out in a cyclic simple shear apparatus. In: E3S web of conferences, vol. 92. EDP Sciences, p 08002
24. Mele L, Lirer S, Flora A (2019b) The effect of densification on Pieve di Cento sands in cyclic simple shear tests. In: National conference of the researchers of geotechnical engineering. Springer, Cham, pp 446–453
25. Mele L, Lirer S, Flora A (2022) An energetic interpretation of liquefaction laboratory tests on partially saturated soils. J Geotechn Geoenviron Eng 148(10):04022082. https://doi.org/10.1061/(ASCE)GT.1943-5606.0002881
26. Murthy TG, Loukidis D, Carraro JAH, Prezzi M, Salgado R (2007) Undrained monotonic response of clean and silty sands. Géotechnique 57(3):273–288
27. Okochi Y, Tatsuoka F (1984) Some factors affecting K0 values of sand measured in triaxial 75 cell. Soils Found 24:52–68
28. Porcino D, Caridi G, Ghionna VN (2008) Undrained monotonic and cyclic simple shear behaviour of carbonate sand. Géotechnique 58(8):635–644
29. Randolph MF, Wroth CP (1981) Application of the failure state in undrained simple shear to the shaft capacity of driven piles. Geotechnique 31(1):143–157
30. Roscoe KH (1953) An apparatus for the application of simple shear to soil samples. In: Proceedings of the 3rd ICSMFE, vol 1, pp 186–191
31. Roscoe KH (1970) The influence of strains in soil mechanics. Geotechnique 20(2):129–170
32. Sivathayalan S, Logeswaran P, Manmatharajan V (2014) Cyclic resistance of a loose sand subjected to rotation of principal stresses. J Geotech Geoenviron Eng 141(3):04014113
33. Sze HY, Yang J (2014) Failure modes of sand in undrained cyclic loading: impact of sample preparation. J Geotech Geoenviron Eng 140(1):152–169
34. Viana Da Fonseca A, Soares M, Fourie AB (2015) Cyclic DSS tests for the evaluation of stress densification effects in liquefaction assessment. Soil Dyn Earthq Eng 75:98–111
35. Villet WCB, Sitar N, Johnson KA (1985) Simple shear tests on highly overeonsolidated offshore silts. In: Offshore technology conference. OnePetro
36. Vucetic M, Lacasse S (1982) Specimen size effect in simple shear test. J Geotech Eng Div 108(12):1567–1585
37. Wai D, Manmatharajan MV, Ghafghazi M (2022) Effects of imperfect simple shear test boundary conditions on monotonic and cyclic measurements in sand. J Geotech Geoenviron Eng 148(1). https://doi.org/10.1061/(ASCE)GT.1943-5606.0002682